
HOLISTIC INFORMATION THEORY OF SPATIAL REMOTE SENSING IMAGING

A PREPRINT

 **Jianan PAN***

Advanced Optics Research Laboratory
Chang Guang Satellite Technology Company Ltd.
jnanpan@outlook.com

 **Junbo HAO**

Advanced Optics Research Laboratory
Chang Guang Satellite Technology Company Ltd.
junbohao0413@163.com

Qixiang GAO

Advanced Optics Research Laboratory
Chang Guang Satellite Technology Company Ltd.
gqx17@tsinghua.org.cn

 **Xing ZHONG**

Advanced Optics Research Laboratory
Chang Guang Satellite Technology Company Ltd.
ciomper@163.com

December 22, 2025

ABSTRACT

To address the non-optimal global design caused by the independent optimization of optical lenses, photodetectors, and computational processing subsystems in traditional remote sensing imaging system design, this paper proposes a holistic information theory for spatial remote sensing imaging. This theory integrates the optoelectronic imaging hardware front end and computational reconstruction back end into a unified framework. It establishes a complete spatial imaging chain information transfer model with the objective of obtaining the required effective information. The paper innovatively proposes a quantifiable Modulation Transfer Function (MTF)-Signal-to-Noise Ratio (SNR) product criterion. It demonstrates that the system information transmission ability is determined by the product of MTF and SNR, and that these parameters can compensate for each other to achieve equivalent information transfer. Validation through a high-resolution Earth observation system case shows that under consistent reconstruction mean square error conditions, increasing time delay integration stages reduces optical aperture size and significantly lowers primary mirror mass. Simulations and physical experiments further indicate that by increasing integration time, low-resolution optical systems achieve reconstructed fidelity comparable to high-resolution systems. This verifies that small-aperture optical systems can achieve equivalent imaging performance by enhancing SNR. This theory has been successfully applied in the design of the Jilin-1 satellite constellation, providing a new paradigm for low-cost high-resolution remote sensing systems.

Keywords High-resolution remote sensing · Microsatellite · System design · Holistic approach

1 Introduction

Remote sensing imaging typically refers to using aircraft or satellites equipped with space optical instruments to measure the characteristics of objects on Earth non-contactly, relying on the propagation of light signals Schowengerdt [2006]. Remote sensing imaging provides repeated and consistent observations of the Earth, which are crucial for monitoring environments and human activities. It has a wide range of applications, including transportation, agriculture, and marine environments Guo et al. [2020]. In recent years, with the continuous advancements in satellite remote sensing manufacturing and microchip processing technologies, the resolution of remote sensing data has consistently improved across spatial and spectral dimensions Zhang et al. [2022]. The enhanced spatial resolution significantly increases the value of remote sensing images.

*corresponding email: jnanpan@outlook.com

Based on the concept of diffraction limitation, the resolution of an optical system is determined by its aperture size, which means that achieving higher spatial resolution in space optical systems requires larger aperture sizes. This leads to satellite platforms having greater mass and volume, resulting in increased manufacturing costs. Several approaches have been proposed to alleviate the increasing deployment costs associated with pursuing high spatial resolution in optical systems by enlarging the aperture. The James Webb Space Telescope Sabelhaus and Decker [2004] employs segmented mirror technology Mesrine et al. [2017], which addresses the challenges of manufacturing large aperture mirrors and the inability of rockets to carry such large mirrors by producing in blocks and deploying in folds. Lightweighting of optical-mechanical structures is researched Zhang and Li [2022], like SPICA Roelfsema et al. [2018] utilizing carbon fiber-reinforced plastics to support specific structures, forming a lightweight architecture. Other advanced research which may be applied in space imaging is ongoing. The imaging performance and deployment costs of various systems using a sparse array of mirror elements as the primary mirror of reflective optical systems are explored by Metwally et al. [2021], based on the concept of optical sparse aperture Meinel and Meinel [2002]. The theoretical and manufacturing of large-aperture metalenses are studied by Hao et al. [2022] and Park et al. [2024]. FalconSAT-7 Asmolova et al. [2015] employs diffractive elements as a collecting aperture, significantly reducing the mass and volume of the optical system.

Due to the diffraction of electromagnetic waves during propagation in space, the spatial positions of physical parameters become distorted when non-contact methods are employed to measure optical information from targets. Traditional imaging instruments utilize focusing optical elements to converge wavefronts onto photodetectors, thereby establishing a spatial mapping between objects and images to achieve optical information measurement. In recent years, with continuous advancements in information science, computational imaging Mait et al. [2018] has been widely applied in optoelectronic imaging fields. Distinct from conventional optical systems where spatial mapping relies entirely on optical lenses, computational imaging systems aim to implement spatial mapping through co-designed front-end and back-end strategies. This approach leverages the advantages of information technology while circumventing bottlenecks in optical system design and manufacturing. The first widespread application of computational-optical joint imaging methods can be traced to the pioneering work in Cathey et al. [1984]. After the proposal of the depth-of-field extension technology Dowski Jr and Cathey [1995], which has significant practical applications, this field has gradually gained attention. Modulation in front-end imaging systems often involves hardware modifications. Consequently, fields like microscopy that permit active hardware modulation particularly benefit from computational imaging techniques, such as Fourier ptychography Zheng et al. [2013] and lensless imaging Ozcan and McLeod [2016]. In contrast, remote sensing spatial imaging systems face limited adoption of computational optical technology due to high hardware iteration costs, difficulties in modulating front-end imaging hardware, and engineering inertia. Thus, imaging systems and image processing systems in remote sensing often remain separately designed. The capability of large-scale satellite constellations for repeat Earth observation, combined with the macroscopic nature of remote sensing applications, results in substantially lower temporal resolution requirements compared to microscopy, which operates at sub-second levels Lorenz [2024]. Remote sensing typically maintains daily-level temporal resolution Roy et al. [2021], allowing high-performance image processing techniques to play a more prominent role. Therefore, effectively leveraging computational imaging to organically integrate optoelectronic hardware with image algorithms and achieving optimal imaging performance under constrained engineering costs represents a crucial developmental imperative for remote sensing imaging technology.

As an information transmission system, the ultimate design goal of the remote sensing spatial imaging system is to obtain predetermined information content at the lowest possible cost. Designers typically decompose this goal into several subsystem-level objectives: 1) The optical system is designed, manufactured, and aligned meticulously to achieve optimal imaging performance with a finite aperture; 2) Semiconductor devices and electronic circuits are optimized through design and process technology to minimize image noise contamination to required levels; 3) Degradation compensations including radiometric correction, sharpening, and denoising are implemented to the greatest extent possible in the image processing subsystem. During optical payload manufacturing and remote sensing data production, optimization of these local components is typically performed without considering constraints from other subsystems, or only accounting for immediately adjacent ones. For example, MTF design targets for optical lenses solely focus on meeting specifications at the Nyquist frequency determined by detectors Fiete [1999], and MTF compensation (MTFc) algorithms for mitigating image blur and noise are heuristic or estimated usually Li et al. [2013], Gu et al. [2005]. Although all subsystems are designed to meet performance requirements at minimal cost, combinations of such locally optimal solutions often fail to achieve global optimality. For example, due to the heuristic MTFc algorithm, the improvement in optical system performance does not guarantee enhanced quality in the final processed images. This demonstrates that engineering design generally lacks the property of optimal substructure Papadimitriou and Steiglitz [1998]. Fortunately, because the physical models and stochastic processes governing the imaging system are nearly well-defined, integrating this multidisciplinary design optimization into a monolithic architecture Martins and Lambe [2013] is feasible. For example, the instrument design principles proposed by the French National Centre for Space Studies state that the value of the MTF-SNR product is an important instrument design objective Rosak et al. [2004], Goudy et al. [2002]. and it is widely used in the satellite industry. Additionally, with the development of AI

Table 1: Nomenclature

Symbol	Definition [Unit]
U	Light field [V/m]
(x, y)	2D spatial position coordinates [m]
(u, v)	2D spatial frequency coordinates [m^{-1}]
z	Axial coordinates [m]
\mathbb{R}	Field of Real Numbers
k	Wave vector [m^{-1}]
λ	Wavelength [m]
I	Optical field intensity [W/m^2]
ϵ_0	Vacuum permittivity [$\text{F} \cdot \text{m}^2$]
c	Lightspeed [m/s]
S_x	Field of View [m^2]
S_f	Optical bandwidth [m^{-2}]
H_{orbit}	Satellite orbit altitude [m]
\mathcal{F}	2D Fourier transform operator
SBP	Space-bandwidth product
f	Focal length [m]
Z	Pixel number
Δ	Pixel size
$F/\#$	F-number
p	Photon number
η	Quantum efficiency
t	Integration time [s]
h	Planck constant [J·s]
DN	Digital number
K_{gain}	Mapping gain from photon to digital number
rect	Window function
comb	Comb function
(m, n)	Discrete coordinates
F	Image spectrum
C	Channel capacity [bit / m^2]
B	Channel bandwidth [m^{-2}]
I_{info}	Maximal mutual information [bit]
SNR	Signal-to-noise ratio
MTF	Modulation transfer function
H	Transfer function
N	Noise spectrum
H_{info}	Information entropy [bit]
n_p	Photon shot noise
E	Expectation
D	Variance
$X \times Y$	The set of spatial position coordinates
$F_u \times F_v$	The set of spatial frequency coordinates
ϵ	Reconstruction error
NPM	Noise power magnification
M	TDI stage

technology in recent years, both MTF and SNR are core metrics for evaluating the effectiveness of intelligent image processing algorithms Ngo et al. [2021], Müller and Braun [2023]. However, theoretical and quantifiable research has not yet been implemented. Therefore, this paper treats the imaging front-end of optical payload cameras and the computational back-end as a unified system. Guided by the objective of obtaining the required effective information, we conduct an optimization analysis for the whole imaging system design. This process involves transformations among optical information, electronic information, and digital information. Consequently, we propose a method called holistic information theory for remote sensing optical design based on this principle. The nomenclature of this section is described in Table 1.

2 Holistic Information Analysis under the Spatial Imaging Chain

For traditional spatial imaging chains, the physical models and stochastic processes are nearly well-defined. However, conventional design methods struggle to ensure globally optimal solutions when combining different subsystems, consequently relying on heuristically proposed principles Zhong et al. [2024]. This section adopts an information-theoretic perspective to examine information transfer throughout the spatial imaging chain, while further investigating how subsystem selections impact systemic information transfer, thus establishing a physical foundation for quantifying holistic information.

2.1 The Propagation of Optical Information

The target information source of remote sensing imaging systems is the radiance of sunlight reflected from ground objects. At any given moment, the acquired information constitutes a two-dimensional light field at the conjugate plane z_{obj} of the detector array, which can be regarded as a linear superposition of plane waves with different propagation directions as

$$U(x, y, z_{obj}) = \iint_{\mathbb{R}^2} A(u, v, z_{obj}) \exp[j2\pi(ux + vy)] dudv, \quad (1)$$

where $A(u, v, z_{obj})$ is the angular spectrum in spatial frequency (u, v) and conjugate plane z_{obj} , $U(x, y, z_{obj})$ is the complex amplitude in spatial position (x, y) and conjugate plane z_{obj} . the free space propagation of the angular spectrum satisfies

$$A(u, v, z_{obj} + \Delta z) = A(u, v, z_{obj}) \exp(jk\Delta z \sqrt{1 - \lambda^2(u^2 + v^2)}) \quad (2)$$

based on the Helmholtz equation. It is evident that the light field itself is bandlimited to $1/\lambda$ when evanescent waves are neglected. Furthermore, although the light field is a spatially continuous physical quantity, the spatially bounded domain over which we can capture it inevitably constrains the information content carried by the observable light field. To quantify the information-carrying capacity of the light field, the space-bandwidth product (SBP) is introduced to measure the information content of the light field Lukosz [1966]. Taking the information carried by the light field intensity $I(x, y) = |U(x, y)|^2/2\epsilon_0 c$ as an example, there is

$$\text{SBP} = S_x S_f. \quad (3)$$

The light field intensity can be represented by this number of independent orthogonal signal components. Moreover, the phase, polarization states, and others of the light field can also carry information.

Returning to the spatial imaging chain, the imaging of the light field through the optical system is affected by the diffraction limit caused by a finite aperture and aberration in engineering implementation. In remote sensing for Earth observation, the light field reflected by ground objects, denoted as U_{obj} , undergoes far-field diffraction over the satellite orbit altitude H_{orbit} , reaches the satellite optical payload, and at this point, the light field U_{in} is proportional to the spectral distribution of U_{obj} as

$$U_{in}(x_{opt}, y_{opt}) \propto \mathcal{F}[U_{obj}(x_{obj}, y_{obj})]. \quad (4)$$

The optical system can often be abstracted as a finite-space light field modulator, which causes the incident light field U_{in} to undergo amplitude modulation A_{ap} due to finite aperture transmission and phase modulation φ_{ap} caused by optical path differences at different spatial positions, and spatial mapping effects resulting in an output light field of

$$U_{out}(x_{opt}, y_{opt}) = U_{in}(x_{opt}, y_{opt}) \cdot \tilde{A}_{ap}(x_{opt}, y_{opt}), \quad (5)$$

where $\tilde{A}_{ap} = A_{ap} \exp[j\varphi_{ap}]$ is the generalized pupil function. Finally, the angular spectrum of the output light field $A_{out}(u, v)$ propagates through a distance of the focal length f , forming the angular spectrum and light field at the image plane. The light intensity detected by the detector is

$$I(x, y) = |\mathcal{F}^{-1}[A_{out}(u, v) \cdot \exp(jkf) \cdot \exp(-j\pi\lambda f(u^2 + v^2))]|^2. \quad (6)$$

Throughout the entire process, the amplitude modulation of the finite aperture leads to the constraint of the target information in the frequency domain, while the finite area of the detector leads to the constraint of the target information in the spatial domain. For traditional circular aperture incoherent imaging systems, the light field bandwidth product reaching the image plane of the detector is

$$\text{SBP}_{\text{opt}} = Z\Delta^2\pi/\lambda^2(F/\#)^2. \quad (7)$$

Moreover, wave aberration causes the complex amplitude of different frequency components in the image to be modulated. However, unlike the cut-off of frequency information caused by a finite aperture, wave aberration only causes attenuation of information, theoretically not leading to information loss.

2.2 Conversion and Digitization of Optoelectronic Information

When the light field reaches the detector, photons will cause the photoelectric effect in the photodiode, exciting electrons to form an electrical signal. Without considering the Poisson process, the photon number p received by the photodetector pixel is determined by its photodetector parameters and light information, as

$$p = \iint_{\Delta \times \Delta} \frac{\eta(\lambda)\lambda\epsilon_0 t I(x, y)}{2h}, \quad (8)$$

where $\Delta \times \Delta$ is the pixel area. The electrical signal induced by the photoelectric effect undergoes amplification with gain K_{gain} and analog-to-digital conversion in the detector circuit, forming the discrete digital image as

$$\text{DN} = \min\{\lceil K_{\text{gain}}p \rceil, \text{DN}_{\text{sat}}\} \quad (9)$$

where $\lceil \cdot \rceil$ is the rounding operation and DN_{sat} is the saturation digital number of the optoelectronic detector, which typically takes the form of $2^N - 1$. In (8), only the intensity of the image field varies with the spatial coordinates. Ignoring the case of overexposure, this equation can be combined with (9) to express the digital number as the form of convolution and sampling as

$$\text{DN}_{\text{img}}(m, n) = k(\lambda)I_{\text{img}}(m\Delta, n\Delta) * \text{rect}(m, n) \cdot \text{comb}(m, n), \quad (10)$$

where $k(\lambda)$ is a spatially independent constant that is related only to the detector parameters and the wavelength of light and $x = m\Delta$. The frequency spectrum of this digital signal is

$$\mathcal{F}[\text{DN}_{\text{img}}(m, n)] = k(\lambda)F_{\text{img}}(u, v) \cdot \text{sinc}(\pi\Delta u, \pi\Delta v) * \text{comb}(\Delta u, \Delta v), \quad (11)$$

where the term $\text{sinc}(\pi\Delta u, \pi\Delta v)$ represents the decay in frequency components caused by window sampling, while the convolution term $\text{comb}(\Delta u, \Delta v)$ results in the periodic extension of the signal spectrum, causing frequency aliasing when the sampling is insufficient. From the bandwidth product perspective, when a signal is sampled and discretized, its spatial domain and frequency domain are coupled. Once the spatial domain characteristics of discrete information are fixed, their frequency domain characteristics are also fixed. Moreover, it can be noticed that, based on the matching criterion of the optical lens and photodetector in remote sensing imaging systems, the optical cut-off frequency is located at 1 to 2 times the Nyquist frequency Fiete [1999], which causes the signals at various spatial frequencies to be often undersampled, thereby reducing the spatial bandwidth product of the discrete information to

$$\text{SBP}_{\text{DN}} = Z. \quad (12)$$

Additionally, due to limitations in detector manufacturing processes, the discretization of the light field is also affected by noise. Considering Shannon's formula

$$C = B\log_2(1 + \text{SNR}), \quad (13)$$

where C is the channel capacity, B is the bandwidth, and SNR is the signal-to-noise ratio of the channel. By applying this formula to spatial imaging scenarios and multiplying both sides by the spatial domain width, we obtain

$$I_{\text{info}}(\text{DN}(m, n); I_{\text{obj}}(x, y)) = \text{SBP}\log_2(1 + \text{SNR}), \quad (14)$$

where I is the maximal mutual information per imaging instance and SBP is the spatial bandwidth product of the system. For example, when the system SNR approaches infinity, the signal received by a single detector is an analog value that cannot be stored with finite-bit precision. Conversely, when quantization noise caused by limited bit depth dominates over photoelectric noise, the image information content corresponds precisely to the raw file size required to store the image.

2.3 Restoration of Digital Information

In information processing systems, methods for image enhancement are typically categorized into 3 classes: 1) Physical model-based methods, which model system degradation and solve inversely to reconstruct images, such as inverse deconvolution reconstruction Schmidt et al. [2013]; 2) Information enhancement-based methods, which heuristically amplify effective components of images, such as edge sharpening and filter-based denoising He et al. [2012]; 3) Learning-based methods, which enhance images by incorporating mega data priors, such as generative adversarial networks Zhang et al. [2018]. Compared to the latter two, the restoration approach of the former relies on system parameters to maximally preserve real information. This type of method models the optoelectronic imaging model as

$$F_{\text{img}}(u, v) = F_{\text{obj}}(u, v)H(u, v) + N(u, v). \quad (15)$$

It integrates the degradation of the system into a degradation kernel $H(u, v)$ and integrates photoelectric noise into degradation noise $N(u, v)$, meaning that images obtained through photoelectric imaging systems are often blurred and noisy. The inverse model of (15) is

$$I_{\text{rec}}(x, y) = \mathcal{F}^{-1}\left[\frac{F_{\text{img}}(u, v) - N(u, v)}{H(u, v)}\right], \quad (16)$$

where I_{rec} is the reconstruction information corresponding to objects based on the image. The spatial domain form $I_{\text{img}}(x, y) - n(x, y)$ of the term $F_{\text{img}}(u, v) - N(u, v)$ in this equation is essentially a severely ill-posed denoising problem, where shot noise caused by the quantum property of photons Gow et al. [2007] dominates the photoelectric noise. Even if photoelectric parameters can be precisely calibrated, the noise impact cannot be eliminated. Under a naive inverse filtering model, both the effective signal and noise are amplified proportionally, thus their information content remains unchanged. However, calibration or estimation of the system degradation kernel $H(u, v)$ inevitably contains errors, leading to erroneous modulation in signal reconstruction, which in turn generates artifacts degrading image quality, such as ringing effects Fergus et al. [2006]. On one hand, this causes certain textures to be abnormally amplified, particularly in frequency bands with low MTF. If these textures are regarded as residual noise after restoration, then the information content of the signal is reduced after restoration. On the other hand, to suppress the abnormal amplification of textures, some regularization terms, such as high-frequency suppression Vaseghi [1996] and local smoothing Jiang et al. [2021], are proposed, trading computational cost and loss of information content for mitigating the signal-to-noise ratio degradation due to abnormal amplification.

In summary, the entire information transmission chain adheres to the principle of data processing inequality, meaning that information progressively diminishes throughout processing stages as

$$H_{\text{info}}[I_{\text{rec}}(x, y)] \leq H_{\text{info}}[I_{\text{img}}(x, y)] \leq H_{\text{info}}[I_{\text{obj}}(x, y)]. \quad (17)$$

Consequently, the information obtainable by photoelectric systems constitutes the upper bound of the restored information

The task of the holistic information transmission chain can be decoupled as follows: 1) The photoelectric imaging hardware system aims to maximize the preservation of light field information content; 2) The image restoration algorithm system aims to recover target light field information as completely as possible, leveraging the photoelectric imaging system parameters and acquired information.

3 Design Methodology based on Holistic Information Analysis

In previous studies, a qualitative principle indicates that for frequencies within the optical cut-off, higher MTF values result in smaller restoration errors under identical noise levels and kernel error spectra Zhong et al. [2024]. Therefore, for frequency bands of interest, systems should be designed with MTF exceeding a certain threshold to counteract restoration errors induced by kernel measurement errors, while maximizing SNR to mitigate noise amplification during restoration. The conclusion that improving MTF and SNR enhances system performance is evident Rosak et al. [2004], Goudy et al. [2002]. In this section, we establish a quantitative functional relationship demonstrating that the information transmittable by photoelectric imaging systems and the restoration accuracy of process systems increases monotonically with the product of MTF and SNR.

3.1 MTF-SNR Product Criteria: Imaging Systems

To establish MTF and SNR design criteria, begin by analyzing information transfer within the hardware system. (14) assumes channel corruption by Gaussian white noise, while in photoelectric imaging systems with the systemic noise such as nonuniform response being well-calibrated, the channel is predominantly contaminated by Poisson noise. Under

sufficient illumination, the instantaneous photon count reaching a specific pixel region on the photodetector array approximates Hayman et al. [2022]

$$p(x, y) + n_p(x, y) \sim \mathcal{N}(p(x, y), p(x, y)), \quad (18)$$

where $n_p(x, y)$ is shot noise caused by light quantum fluctuations and \mathcal{N} is the Gaussian distribution. The statistical characteristics of the shot noise spectrum $N_p(u, v)$ are

$$E[N_p(u, v)] = 0, D[N_p(u, v)] = \sum_{(x, y) \in X \times Y} p(x, y). \quad (19)$$

Therefore, the shot noise can be approximated as white noise influenced by the entire signal. Furthermore, the spectrum of shot noise, formed by the linear sum of Gaussian noises obeying different means and variances, follows a complex Gaussian distribution. Assuming the signal spectrum is also complex Gaussian distributed, it satisfies the Gaussian channel information capacity formulation. However, the information capacity of individual frequency band channels varies with overall signal fluctuations. To investigate information transfer in the photoelectric process, consider the signal power spectrum as

$$E[|F(u, v)|^2] = \left| \sum_{(x, y) \in X \times Y} \exp[-j2\pi(ux + vy)] p(x, y) \right|^2, \quad (20)$$

which makes the SNR in each spectrum be

$$\text{SNR}(u, v) = \sqrt{\frac{|\sum_{(x, y) \in X \times Y} \exp[-j2\pi(ux + vy)] p(x, y)|^2}{\sum_{(x, y) \in X \times Y} p(x, y)}}. \quad (21)$$

When p increases by a factor of m , the SNR across all frequency bands increases by the factor \sqrt{m} . This equally applies to the digital signal obtained after light quanta pass through gain K . Furthermore, the SNR in different frequency bands depends on the signal itself, and the optical imaging channel modulates the complex amplitude of the signal. Consequently, at the entire system level, there is

$$I_{\text{info}}(I_{\text{img}}(x, y); I_{\text{obj}}(x, y)) = \sum_{(u, v) \in F_u \times F_v} \log_2(1 + \text{MTF}(u, v) \cdot \text{SNR}(u, v)), \quad (22)$$

where $X \times Y$ is the set of spatial position coordinates, $F_u \times F_v$ is the set of spatial frequency coordinates, and

$$|X \times Y| = |F_u \times F_v| = Z. \quad (23)$$

It integrates the frequency response capability and signal fidelity capability of the imaging system to characterize the information transfer capacity of the imaging channel. In previous research, the MTF-SNR Product (MSP) factor was typically used as a heuristic design metric Fiete [1999], but it is fundamentally directly correlated with the information transfer capacity of the imaging channel.

In photoelectric imaging hardware systems, consistent MSP can achieve equivalent information. This implies that when design objectives for a spatial system are fixed particularly in high-resolution spatial systems requiring large optical aperture specifications, one may enhance the SNR through increased integration stages or satellite attitude adjustments for staring imaging Lian et al. [2017], thereby relaxing demands on optical system performance.

Approximately, for a high-performance baseline system and an optimized system, based on (22) and the conclusion that SNR is frequency-domain independent, the system should elevate SNR to

$$\text{SNR} \approx \text{SNR}_{\text{base}} \left[\prod_{(u, v) \in F_u \times F_v} \frac{\text{MTF}_{\text{base}}(u, v)}{\text{MTF}(u, v)} \right]^{1/Z} \quad (24)$$

or employ parameter scanning to compute numerical solutions for implicit equation (22) to obtain more precise SNR values.

3.2 MTF-SNR Product Criteria: Information Restoration

At the system level, a consistent MSP level ensures that the upper bound of information obtainable by the system remains consistent. However, consistent channel capacity does not guarantee consistent information acquisition because this also depends on the information input, so the fidelity of information transmission is a critical performance attribute of the system. From a computational restoration perspective, for a specific MSP level and disregarding core errors, inverse

filtering restoration achieves complete preservation of information and reaches the upper bound of the information inequality (17), because the SNR and SBP remain unchanged. Set the spectrum of white noise to N_f across all frequency bands. When inverse filtering restoration is applied, the absolute mean square error (MSE) of the information is given by

$$|\varepsilon|^2 = \frac{|N_f|^2}{Z} \sum_{(u,v) \in F_u \times F_v} \frac{1}{\text{MTF}^2(u,v)}. \quad (25)$$

Clearly, the noise power magnification (NPM) can be defined as

$$\text{NPM} = \frac{1}{Z} \sum_{(u,v) \in F_u \times F_v} \frac{1}{\text{MTF}^2(u,v)}, \quad (26)$$

which characterizes the amplification ratio of noise power during reconstruction. For the baseline system and the optimized system, to ensure the consistency of information restoration performance,

$$\text{SNR}/\sqrt{\text{NPM}} = \text{SNR}_{\text{base}}/\sqrt{\text{NPM}_{\text{base}}} \quad (27)$$

should be held. It differs from the form of (24) because (24) characterizes the maximum transmittable information of the optical system whereas (27) characterizes the actual information transmitted by the optical system in an imaging task. These respectively represent task-agnostic system channel capability and task-dependent target information. The system with high channel capability preserves more raw physical features potentially irrelevant to the current task, which can provide foundational support for downstream tasks such as super-resolution algorithms Pan et al. [2025].

In image restoration tasks, based on different prior assumptions, the restoration process maximizes the corresponding objective function at the expense of physical information. For instance in Wiener filtering with an additional low-pass filter, the absolute MSE of the information is given by

$$|\varepsilon|^2 \approx \frac{1}{Z} \left(\sum_{(u,v) \in F_u \times F_v} \frac{|N_f|^2 Lp^2(u,v)}{\text{MTF}^2(u,v)} + 2 \sum_{(u,v) \in F_u \times F_v} F_{\text{obj}}(u,v) \overline{Lp}(u,v) \times \sum_{(u,v) \in F_u \times F_v} \frac{|N_f| Lp(u,v)}{\text{MTF}(u,v)} \right), \quad (28)$$

where

$$Lp(u,v) = \frac{1}{1 + 1/[\text{MTF}(u,v) \cdot \text{SNR}(u,v)]^2}. \quad (29)$$

As the frequency band increases, the reduction in the MTF value causes the enhancement of low-pass filtering. Compared to (25), the first term of (28) adds a noise suppression term from low-pass filtering but relatively the latter term causes damage to the information. In fact, all restoration formulas possessing the form of

$$F_{\text{rec}} = \text{argmin}_{F_{\text{obj}}} \|HF_{\text{obj}} - F_{\text{img}}\|_2^2 + \lambda P(F_{\text{obj}}) \quad (30)$$

have consistent restored MSE form expressed in the form of

$$|\varepsilon|^2 \approx \frac{1}{Z} \left(\sum_{(u,v) \in F_u \times F_v} \frac{|N_f|^2}{\text{MTF}^2(u,v)} + 2 \frac{\lambda}{\text{MTF}^2(u,v)} \frac{\partial P(F_{\text{obj}})}{\partial F_{\text{obj}}} \Big|_{F_{\text{obj}}=\hat{F}_{\text{obj}}} \sum_{(u,v) \in F_u \times F_v} \frac{|N_f|}{\text{MTF}(u,v)} \right), \quad (31)$$

where H is the optical transfer function (OTF) and P is the prior function of the image. So based on the specific task requiring information, a trade-off should be made between the maximum obtainable information and the fidelity of the information.

3.3 System Design Based on MTF-SNR Product Criteria

Based on the analysis of holistic information in previous sections, we can abstract a system design to

$$\begin{aligned} & \max \lambda_I I + \lambda_E E \\ & \text{s.t. } I = \sum_{(u,v) \in F_u \times F_v} \log_2(1 + \text{MTF}(u,v) \cdot \text{SNR}(u,v)), \\ & E = - \sum_{(u,v) \in F_u \times F_v} |\varepsilon(u,v)|^2 \end{aligned} \quad (32)$$

where λ_I and λ_E should be determined by the specific task to favor signals containing more true information or signals more similar to the original signal. Considering engineering requirements, when requirements are specified, there should be

$$\begin{aligned} & \min \lambda_{\text{MTF}} \text{MTF} + \lambda_{\text{SNR}} \text{SNR} \\ & \text{s.t. } E \geq E_{\text{base}}, \end{aligned} \quad (33)$$

where MTF and SNR are determined by the system while λ_{MTF} and λ_{SNR} are determined by the cost of improving the MTF and SNR respectively. It is often not formalized in design processes but it embodies the core design concept. When designing a space system with the smallest possible aperture, there should be $\lambda_{\text{SNR}} \ll \lambda_{\text{MTF}}$. In other words, under the imaging and restoration requirements, the reduction in MTF can be compensated by improving SNR to complete the system design.

Table 2: Main space system parameters

Parameter	Symbol	Value
Orbit altitude	H_{orbit}	500 km
Orbit inclination	i_{orbit}	98° sun synchronous
Atmospheric model	-	Mid-latitude summer
Pixel size	Δ	10 μm
Pixel number	Z	4096 \times 4096
TDI stage	M	8~128
Full well	p_{FW}	250 ke-
Quantum efficiency	η	about 50%
Line frequency	f_L	30 kHz
Quantization bits	-	12 bit
Spectral band	λ	400 nm ~ 900 nm

4 Design Case based on Holistic Information Theory

4.1 Benchmark System

The primary technology for high-resolution optical remote sensing imaging remains large-aperture monolithic optical remote sensing imaging systems. Considering aperture design for a space optical system on a small satellite, the satellite platform, atmospheric environment, and photodetector parameters adopt reasonable values as shown in Table 2 Attia et al. [2020]. Under these parameters, the design target achieves a ground sampling distance (GSD) of 0.1 m in the visible band. This determines the optical focal length F as 50 m and the Nyquist frequency f_{Nyq} as 50 lp/mm. If the catadioptric configuration is selected for the space optical system and diffraction-limited performance is achievable, this indicates the pupil function is a circular amplitude modulation function. Based on the central wavelength and conventional design specifications of $\text{MTF@Nyq} \geq 0.3$, the optical aperture is determined to be approximately 2800 mm. When the system receives sufficient uniform radiation at 0° solar zenith angle and 0° satellite zenith angle, the SNR reaches about 100 at $\rho = 0.2$ using 16-stage integration Van Achteren et al. [2006], where ρ denotes ground reflectance, assigned a common value of 0.2 Berk et al. [2014]. Without loss of generality, inverse filtering restoration is applied for fundamental system analysis. Based on (26), the NPM of this system can be calculated as 8.56, meaning that after image reconstruction, the noise level will be amplified to approximately 3 times.

4.2 Design of Small Aperture Imaging System

In Section 4.1, to achieve high-resolution remote sensing, its optical aperture needs to reach 2800 mm, leading to a large mechanical envelope size. The mass of the optical system often increases with the cube of its outer diameter Cheng [2009], greatly increasing the deployment cost of the satellite due to its size and mass, which poses a challenge for the construction of large-scale constellations. Reducing the primary mirror size is the most direct means to reduce engineering costs, therefore we analyze based on the mathematical model proposed in Section 3.3 for the requirements in Section 4.1.

In Section 3, we demonstrated that the MSP is the decisive factor affecting information acquisition and restoration in imaging systems. This suggests that we can enhance tolerance to image quality degradation by improving the SNR. Under sufficient radiation, the factors affecting SNR in imaging systems are the area of the optical aperture and the integration time, respectively by increasing the area receiving radiation and the time to increase the photons received by the detector as

$$\text{SNR} = \frac{\Delta \sqrt{\pi \int_{\lambda_{\min}}^{\lambda_{\max}} \eta(\lambda) (\lambda/hc) (M/f_L) L(\lambda) \tau(\lambda) d\lambda}}{2F/\#}, \quad (34)$$

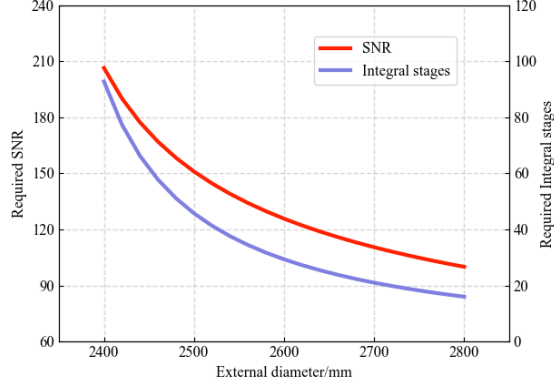


Figure 1: The required SNR and integration stages vary with optical aperture to maintain an equal level of MSE in the reconstructed image.

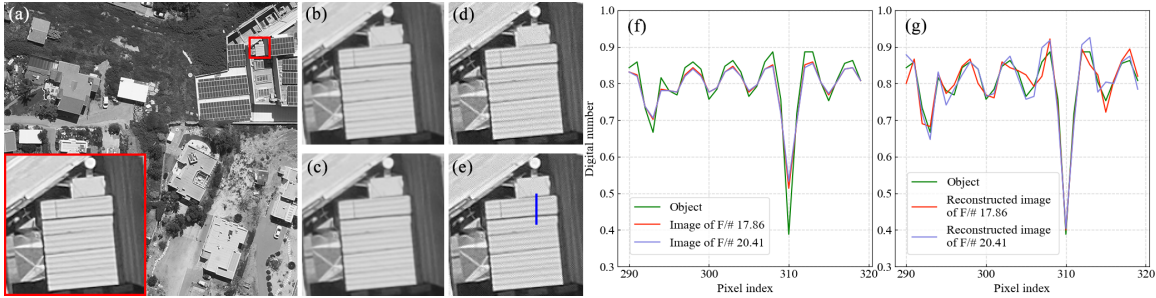


Figure 2: Simulated imaging and computational reconstruction results of the same target object under a high-MTF, low-SNR system and a low-MTF, high-SNR system. The target object used in the simulation experiment and the region of interest labeled by red box is shown in (a). The images of the target region with the two systems is shown in (b) and (c). The reconstructed images based on system parameters and the images is presented in (d) and (e). The grayscale values of periodic textures labeled by the blue line within the target regions is illustrated in (f) and (g). The system with a higher F-number produces images with lower contrast of the target texture, but after reconstruction, both images maintain consistent contrast and fidelity.

where $L(\lambda)$ and $\tau(\lambda)$ denote the irradiance in the entrance aperture and the transmittance of the optical system at a specific wavelength respectively. By adjusting the integration stages of the detector, the degradation of MTF and SNR due to aperture reduction can be compensated. Therefore, we gradually reduced the aperture of the optical system and observed the changes in the required integration stages to maintain the same level of reconstruction error, as shown in Fig. 1. When electronic pressure is low, integration time can greatly alleviate the demand for the optical aperture. For example, using 64 integration stages allows reducing the optical aperture to 2450 mm, with the envelope size and mass of the primary mirror decreasing by approximately 20% and 30% respectively based on Cheng [2009].

4.3 Simulation and Imaging Experiments

To verify the theoretical correctness of the design in Section 4.2, we conducted a simulation experiment. We selected a high-definition image as the target object, shown in Fig. 2(a). First, using the parameters from Section 4.2, we applied optical degradation under paraxial approximation with F/# values of 17.86 and 20.41, and added Poisson noise at SNR levels of 100 and 170 under saturated grayscale to give images of the target object. We focused on a texture-rich region and the images are shown in Fig. 2(b) and 2(c). Next, using the correct blur kernels, we performed inverse filtering reconstruction to get the reconstructed images for regions 2(d) and 2(f). The PSNR representing the MSE of reconstruction for these two reconstructed images is 33.79 and 33.68, showing consistent restoration quality.

Additionally, we conducted a physical experiment. We modified the MTF and SNR by changing the aperture of the optical lens and the exposure time of the detector. Here, adjusting the aperture results in F-numbers of 2.8 and 16 for the optical lens. The pixel size is $6.45 \mu\text{m}$, and the center wavelength of the narrowband LED light source is 532 nm. We adjusted the exposure times for the two experiments to make the imaging grayscale reach half-saturation. Based on (26),

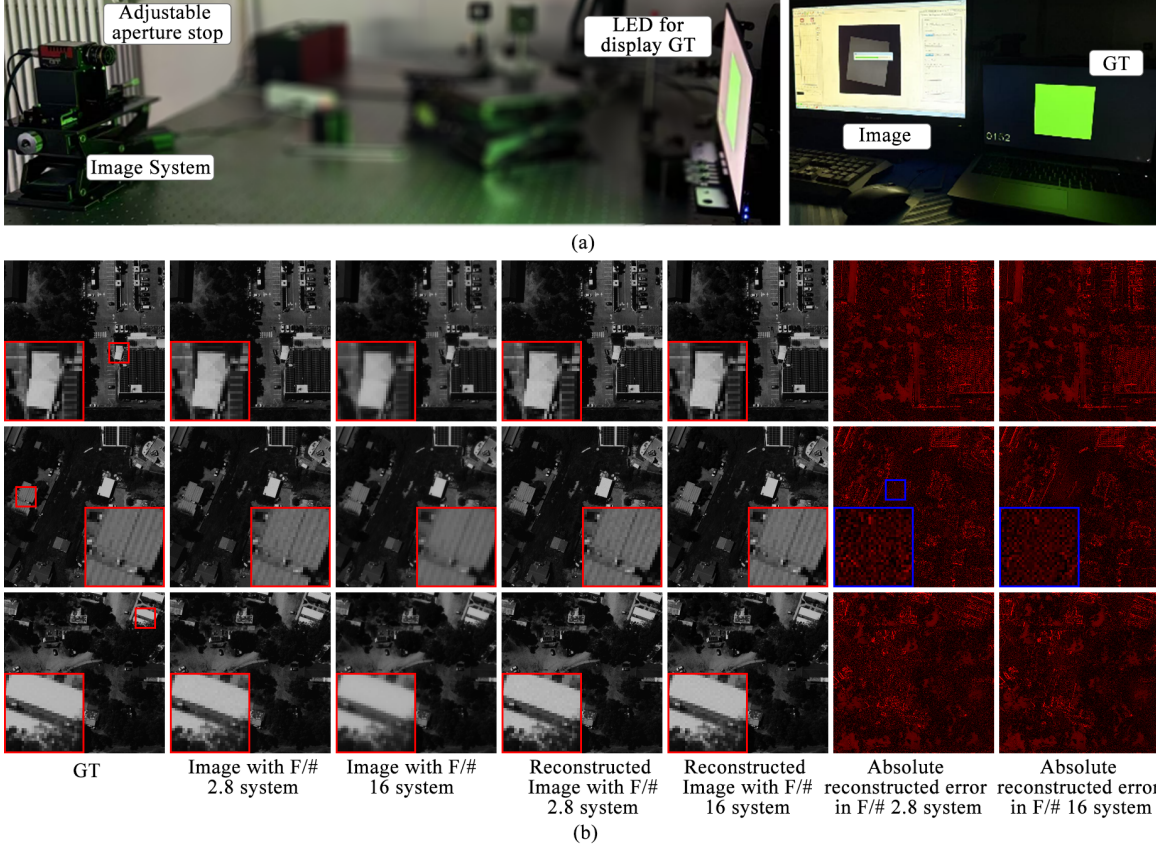


Figure 3: Experimental setup and results. Figure (a) shows the experimental setup, where the grayscale-to-radiance mapping relationship for the LED and the non-uniform response of the camera are calibrated as much as possible. Figure (b) shows the experimental results, examining the PSNR of reconstructed images for three targets. The PSNR values are 49.91, 50.50, and 50.37 in the F/# 2.8 system, respectively, while there are the values of 50.42, 50.67, and 50.92 in the F/# 16 system. The reconstruction quality of both systems was basically maintained at an equivalent level. Please zoom in to observe pixel level details.

the NPM values for the F/# 2.8 and F/# 16 systems are 1.28 and 23.64, respectively. Then, according to (27), the SNR of the F/# 16 system should be about 4.3 times that of the F/# 2.8 system. Therefore, the F/# 16 shooting is extended to 18 times. The entire imaging system was well-calibrated. The experiment and results are shown in Fig. 3. Each column represents one target. The blur levels of the images are very different between the two systems. However, after reconstruction, the similarity to GT was basically consistent. In the reconstructed image of the F/# 2.8 system, noise was amplified more uniformly. In contrast, in the F/# 16 system, high-frequency noise was amplified more severely, resulting in it shows a grid-like noise texture as shown in the absolute reconstructed error in Fig. 3(b). Additionally, due to residual systematic errors in calibration, there are edge textures and grayscale bias in the reconstruction error, but this is consistent for both systems and does not affect the conclusion.

In summary, when the imaging and computational restoration system is considered as a whole, the MTF and SNR of the imaging system, as limitations on information transmission, can compensate for each other to achieve consistent computational imaging results. This means that for high-resolution remote sensing imaging requirements, the requirements for large-aperture and high-precision lens fabrication can be relaxed. Instead, compensation can be achieved through the fine design of photoelectric detectors and the staring imaging method to meet the set imaging performance targets.

5 Conclusion and Future Work

This paper proposes the concept of holistic information imaging, which jointly considers the optical subsystem, electronic subsystem, and computational subsystem of an imaging system. This establishes quantitative criteria for collaboration between these subsystems. Specifically, for standard monolithic remote sensing imaging systems, we

demonstrate through theoretical analysis and experimentation that system design can relax MTF requirements by improving SNR. This avoids the requirements for large-aperture lenses and high-precision surface fabrication. This theory has been applied to the development of the Jilin-1 constellation satellites, enabling ultra-high-resolution Earth remote sensing at acceptable manufacturing costs.

However, this work still faces challenges. First, while we analyze the information transmission chain in holistic information imaging, the advantages of increased information capacity need validation across diverse application scenarios. Thus, investigating broader interactions between computational algorithms and imaging systems remains a key future task. Additionally, the uncertainty in degradation calibration during imaging is an important problem affecting engineering applications. Finally, wider imaging paradigms like hybrid refractive-diffractive optical systems and metalens systems can also be treated as information transmission systems. Integrating all imaging systems into a unified framework constitutes another critical future direction.

References

- Robert A Schowengerdt. *Remote sensing: models and methods for image processing*. elsevier, 2006.
- Huadong Guo, Michael F Goodchild, and Alessandro Annoni. *Manual of digital Earth*. Springer Nature, 2020.
- Bing Zhang, Yuanfeng Wu, Boya Zhao, Jocelyn Chanussot, Danfeng Hong, Jing Yao, and Lianru Gao. Progress and challenges in intelligent remote sensing satellite systems. *IEEE Journal of Selected Topics in Applied Earth Observations and Remote Sensing*, 15:1814–1822, 2022.
- Phillip A Sabelhaus and John E Decker. An overview of the james webb space telescope (jwst) project. *Optical, Infrared, and Millimeter Space Telescopes*, 5487:550–563, 2004.
- M Mesrine, E Thomas, S Garin, P Blanc, C Alis, F Cassaing, and D Laubier. High resolution earth observation from geostationary orbit by optical aperture synthesis. In *International Conference on Space Optics—ICSO 2006*, volume 10567, pages 71–77. SPIE, 2017.
- Changhao Zhang and Zongxuan Li. A review of lightweight design for space mirror core structure: Tradition and future. *Machines*, 10(11):1066, 2022.
- Peter R Roelfsema, Hiroshi Shibai, L Armus, D Arrazola, M Audard, MD Audley, CM Bradford, I Charles, P Dieleman, Y Doi, et al. Spica—a large cryogenic infrared space telescope: unveiling the obscured universe. *Publications of the Astronomical Society of Australia*, 35:e030, 2018.
- Mohamed Metwally, Fawzy Eltohamy, and Taher M Bazan. Design of very high-resolution satellite telescopes part iii: Telescope size reduction. *IEEE Transactions on Aerospace and Electronic Systems*, 57(6):4044–4050, 2021.
- Aden Baker Meinel and Marjorie Pettit Meinel. Large sparse-aperture space optical systems. *Optical Engineering*, 41(8):1983–1994, 2002.
- Junbo Hao, Ting Ma, Zilin Ye, Chen Chen, Dahai Yang, Keya Zhou, Yiqun Wang, Peng Jin, and Jie Lin. Simulation for multiwavelength large-aperture all-silicon metalenses in long-wave infrared. *Nanotechnology*, 33(22):225203, 2022.
- Joon-Suh Park, Soon Wei Daniel Lim, Arman Amirzhan, Hyukmo Kang, Karlene Karrfalt, Daewook Kim, Joel Leger, Augustine Urbas, Marcus Ossiander, Zhaoyi Li, et al. All-glass 100 mm diameter visible metalens for imaging the cosmos. *ACS nano*, 18(4):3187–3198, 2024.
- Olha Asmolova, Geoff Andersen, Matthew G McHarg, Trey Quiller, Carlos Maldonado, and Thomas Dickinson. Design and test of a novel solar imaging payload for small satellites. In *UV/Optical/IR Space Telescopes and Instruments: Innovative Technologies and Concepts VII*, volume 9602, pages 159–166. SPIE, 2015.
- Joseph N Mait, Gary W Euliss, and Ravindra A Athale. Computational imaging. *Advances in Optics and Photonics*, 10(2):409–483, 2018.
- W Thomas Cathey, B Roy Frieden, William T Rhodes, and Craig K Rushforth. Image gathering and processing for enhanced resolution. *Journal of the Optical Society of America A*, 1(3):241–250, 1984.
- Edward R Dowski Jr and W Thomas Cathey. Extended depth of field through wave-front coding. *Applied optics*, 34(11):1859–1866, 1995.
- Guoan Zheng, Roarke Horstmeyer, and Changhuei Yang. Wide-field, high-resolution fourier ptychographic microscopy. *Nature photonics*, 7(9):739–745, 2013.
- Aydogan Ozcan and Euan McLeod. Lensless imaging and sensing. *Annual review of biomedical engineering*, 18(1):77–102, 2016.
- Ulrich J Lorenz. Microsecond time-resolved cryo-electron microscopy. *Current Opinion in Structural Biology*, 87:102840, 2024.

- David P Roy, Haiyan Huang, Rasmus Houborg, and Vitor S Martins. A global analysis of the temporal availability of planetscope high spatial resolution multi-spectral imagery. *Remote Sensing of Environment*, 264:112586, 2021.
- Robert D Fiete. Image quality and $[\lambda]^{fn/p}$ for remote sensing systems. *Optical Engineering*, 38(7):1229–1240, 1999.
- Xiaoying Li, Xingfa Gu, Qiaoyan Fu, Tao Yu, Hailiang Gao, Jianguo Li, and Li Liu. Removing atmospheric mtf and establishing an mtf compensation filter for the hj-1a ccd camera. *International Journal of Remote Sensing*, 34(4):1413–1427, 2013.
- Xingfa Gu, Xiaoying Li, Xiangjun Min, Tao Yu, Jijuan Sun, Yong Zeng, Hua Xu, and Ding Guo. In flight mtf monitoring and compensation for ccd camera on cbers-02. *Science in China Series E Engineering & Materials Science*, 48 (Suppl 2):29–43, 2005.
- Christos H Papadimitriou and Kenneth Steiglitz. *Combinatorial optimization: algorithms and complexity*. Courier Corporation, 1998.
- Joaquim RRA Martins and Andrew B Lambe. Multidisciplinary design optimization: a survey of architectures. *AIAA journal*, 51(9):2049–2075, 2013.
- A Rosak, C Latry, V Pascal, and D Laubier. From spot 5 to pleiades hr: evolution of the instrumental specifications. In *5th International Conference on Space Optics*, volume 554, pages 141–148, 2004.
- Philippe Goudy, Philippe Kubik, Bernard Rouge, and Christophe Latry. From image processing concepts to instrument design in remote sensing satellites. In *2002 11th European Signal Processing Conference*, pages 1–4. IEEE, 2002.
- Tan D Ngo, Tuyen T Bui, Tuan M Pham, Hong TB Thai, Giang L Nguyen, and Tu N Nguyen. Image deconvolution for optical small satellite with deep learning and real-time gpu acceleration. *Journal of Real-Time Image Processing*, 18 (5):1697–1710, 2021.
- Patrick Müller and Alexander Braun. Mtf as a performance indicator for ai algorithms? *Electronic Imaging*, 35:1–7, 2023.
- Xing Zhong, Jianan Pan, and Qixiang Gao. Effects of aperture shapes on imaging spatial quality from end-to-end perspective. *Optics and Lasers in Engineering*, 183:108538, 2024.
- W Lukosz. Optical systems with resolving powers exceeding the classical limit. *Journal of the Optical Society of America*, 56(11):1463–1471, 1966.
- Uwe Schmidt, Carsten Rother, Sebastian Nowozin, Jeremy Jancsary, and Stefan Roth. Discriminative non-blind deblurring. In *Proceedings of the IEEE conference on computer vision and pattern recognition*, pages 604–611, 2013.
- Kaiming He, Jian Sun, and Xiaoou Tang. Guided image filtering. *IEEE transactions on pattern analysis and machine intelligence*, 35(6):1397–1409, 2012.
- Yungang Zhang, Yu Xiang, and Lei Bai. Generative adversarial network for deblurring of remote sensing image. In *2018 26th International Conference on Geoinformatics*, pages 1–4. IEEE, 2018.
- Ryan D Gow, David Renshaw, Keith Findlater, Lindsay Grant, Stuart J McLeod, John Hart, and Robert L Nicol. A comprehensive tool for modeling cmos image-sensor-noise performance. *IEEE Transactions on Electron Devices*, 54 (6):1321–1329, 2007.
- Rob Fergus, Barun Singh, Aaron Hertzmann, Sam T Roweis, and William T Freeman. Removing camera shake from a single photograph. In *Acm Siggraph 2006 Papers*, pages 787–794. 2006.
- Saeed V Vaseghi. Wiener filters. In *Advanced Signal Processing and Digital Noise Reduction*, pages 140–163. Springer, 1996.
- Shikai Jiang, Xiyang Zhi, Wei Zhang, Dawei Wang, Jianming Hu, and Wenbin Chen. Remote sensing image fine-processing method based on the adaptive hyper-laplacian prior. *Optics and Lasers in Engineering*, 136:106311, 2021.
- Matthew Hayman, Willem J Marais, Hristo G Chipilski, Robert A Stillwell, and Scott M Spuler. When can poisson random variables be approximated as gaussian? In *International Laser Radar Conference*, pages 133–139. Springer, 2022.
- Yijun Lian, Yudong Gao, and Guoqiang Zeng. Staring imaging attitude control of small satellites. *Journal of Guidance, Control, and Dynamics*, 40(5):1278–1285, 2017.
- Jianan Pan, Chunfeng Zhang, Xiaojun He, Xing Zhong, and Ye Lan. Digital super-resolution for tdi remote sensing via micro-misaligned pushbroom imaging and computational reconstruction. *ISPRS Journal of Photogrammetry and Remote Sensing*, 227:733–744, 2025.

- Walid A Attia, Fawzy Eltohamy, and Taher M Bazan. Design of very high resolution satellite telescopes part ii: comprehensive performance assessment. *IEEE Transactions on Aerospace and Electronic Systems*, 56(5):4049–4055, 2020.
- T Van Achteren, B Delauré, and J Everaerts. Instrument design for the pegasus hale uav payload. *International Archives of Photogrammetry, Remote Sensing and Spatial Information Sciences*, 2006.
- Alexander Berk, Patrick Conforti, Rosemary Kennett, Timothy Perkins, Fred Hawes, and Jeannette Van Den Bosch. Modtran® 6: A major upgrade of the modtran® radiative transfer code. In *2014 6th Workshop on Hyperspectral Image and Signal Processing: Evolution in Remote Sensing (WHISPERS)*, pages 1–4. IEEE, 2014.
- Jingquan Cheng. The principles of astronomical telescope design. 2009.